Astron. Astrophys. 342, 592–600 (1999)

ASTRONOMY AND ASTROPHYSICS

Latitudinal properties of the Lyman α and O VI profiles in the extended solar corona

L. Zangrilli[1,2], **P. Nicolosi**[1,2], **G. Poletto**[3], **G. Noci**[4], **M. Romoli**[3], **and J.L. Kohl**[5]

[1] Dipartimento di Ingegneria Elettronica ed Informatica, Università degli Studi di Padova, I-35131 Padova, Italy
[2] Istituto Nazionale per la Fisica della Materia, Unità di Padova, Italy
[3] Osservatorio Astrofisico di Arcetri, I-50125 Firenze, Italy
[4] Università di Firenze, I-50125 Firenze, Italy
[5] Harvard-Smithsonian Center for Astrophysics, Cambridge, MA 02138, USA

Received 15 September 1998 / Accepted 9 November 1998

Abstract. We have analysed the latitudinal properties of the profiles of the H I Lyman α line at 1215.6 Å and of the O VI doublet at 1031.9 Å and 1037.6 Å in the extended solar corona, between $1.5\,\mathrm{R}_\odot$ and $2.0\,\mathrm{R}_\odot$. Observations have been performed with the UltraViolet Coronagraph Spectrometer (UVCS) on board the ESA-NASA solar satellite SOHO (SOlar and Heliospheric Observatory). The results show that these lines have quite a different behaviour with latitude: the Ly α line has larger full width at half maximum (FWHM) values in the streamer region and narrower ones towards polar latitudes, while the O VI lines have a minimum FWHM at the center of the streamer, which almost steadily increases towards polar regions. The observations have been analysed looking also for an interpretation in terms of selective heating mechanisms. The implications of our results for coronal heating theories are also examined. In particular we discuss the possibility for the presence of the ion-cyclotron coronal heating mechanism. Moreover, we point out an interesting correlation between the intensity of the coronal lines and their widths, which may be relevant to the open question of the different morphological features visible in the Ly α and O VI lines.

Key words: line: profiles – Sun: corona – Sun: solar wind – Sun: UV radiation

1. Introduction

1.1. Purpose of the research

The purpose of the present research is to study some basic properties of the H I Lyman α and O VI line profiles in the extended solar corona, as a function of latitude and heliocentric distance. The coronal Ly α emission originates from resonant scattering of the chromospheric radiation, while the OVI doublet has, besides the resonant scattering component, a significant collisional contribution (Withbroe et al. 1982; Noci, Kohl, & Withbroe 1987). Spectroscopic observations have been performed with the UVCS spectrometer on board the SOHO spacecraft (Domingo, Fleck, & Poland 1995). From the analysis of these UV lines we derived information about the thermodynamical properties of the coronal medium, averaged along the line of sight. A particularly relevant parameter that can be derived from the line profile is the kinetic temperature of the plasma, defined as (see for example Jefferies 1968)

$$T_\mathrm{k} = \left[\left(\frac{c\Delta\lambda_\mathrm{FWHM}}{1.67\lambda}\right)^2 - \xi^2\right]\frac{M}{2k} \qquad (1)$$

where *c* is the speed of light, λ is the wavelength, $\Delta\lambda_\mathrm{FWHM}$ is the full width at half maximum (FWHM), ξ represents the velocity contribution from non-thermal motions, *M* is the ion mass, *k* is the Boltzmann constant. The kinetic temperature is related to the coronal heating mechanism (see, for instance, Kohl et al. 1998); we plan to study its latitudinal properties through the analysis of the FWHM values of the line profiles of neutral Hydrogen and O VI. Previous UVCS observations of coronal line profiles mainly focussed on their behaviour at different altitudes in either equatorial or polar regions (Kohl et al. 1997; Noci et al. 1997a; Antonucci et al. 1997; Strachan et al. 1997). The results reported in these works will be analytically compared with the present ones in Sect. 4.

Recent works tend to consider coronal heating and solar wind acceleration as related phenomena. Because Ulysses spacecraft observations (Phillips et al. 1995) confirmed that the solar wind is essentially bimodal, being either fast or slow with few values in between, we investigate whether the heating mechanism is bimodal as well.

On the theoretical side few works have addressed so far the problem of the latitudinal variation of the solar wind parameters. A class of exact analytical hydrodynamical and magnetohydrodynamical (MHD) solutions have been presented in a series of works by Lima & Priest (1993), Sauty & Tsinganos (1994), Lima & Tsinganos (1996). In these works the dynamical equations are solved, then a consistent solution for the energy equation is found a posteriori. Analogously, Stewart & Bravo (1997) have recently presented a self-consistent MHD model of the thermally driven solar wind. Numerical models of the solar wind have been developed by Wang et al. (1998) using ad

Send offprint requests to: L. Zangrilli (zangrilli@pd.astro.it)

hoc heat source and momentum terms. Our analysis of the latitudinal properties of the UV coronal line profiles may provide additional constraints to the development of solar wind models.

Special effort has been taken to improve the confidence on the derived data. For this reason a careful evaluation of the statistical and experimental uncertainty of the various measurements has been carried out, taking into account all the instrumental effects which may possibly affect the observed spectra.

1.2. The UVCS spectrometer

The UVCS experiment is a coronagraph spectrometer, designed for ultraviolet spectroscopy and visible light polarimetry, observing the extended solar corona from the inner lagrangian point L1; for a comprehensive description of the intrument see Kohl et al. (1995). Its primary scientific objective is to identify and understand the dominant physical processes operating in the extended solar corona and generating the solar wind. In particular, UVCS is meant to investigate the mechanisms for accelerating the solar wind and heating the coronal plasma, and to locate the coronal sources of the solar wind. The instrument consists of three telescopes with external and internal occultation and a high resolution stigmatic spectrometer assembly. Three spherical telescope mirrors focus co-registered images of the corona onto three entrance slits of the spectrometer assembly. The spectrometer assembly is also composed of three channels. The Ly α channel is a toric grating spectrometer operating in the spectral region 1145–1287 Å and optimized for line profile measurements of the H I line at 1215.6 Å. The O VI channel is similarly a toric grating spectrometer, but operating in the range 984–1080 Å, and optimized for measurements of the O VI lines at 1031.9 Å and 1037.6 Å. The detectors for both channels are two dimensional photon counting, centroiding, microchannel plate (MCP) sensors (Siegmund et al. 1994). The position readout is accomplished by a multilayer crossed delay line anode. The detected image is digitized in an array of 1024 pixels in the spectral direction and 360 in the spatial one. The third channel is a visible light polarimeter, consisting of an entrance aperture, a polarimeter assembly, and a photomultiplier tube. It measures polarized radiance in the band 4500–6000 Å. The three channels observe simultaneously the same portion of solar corona; the slits are normal to the radial direction through their center. Along the slit the spatial coverage of the Ly α and O VI channels is ~ 40 arcmin, while the visible light channel observes only a region of 14 arcsec $\times$ 14 arcsec about the center of the slit. The field of view of UVCS extends from 1.2 to 12 $R_\odot$, and is explored by tilting the primary mirrors. In addition UVCS can be rotated about the sun center, to observe the corona at any position angle. Offset pointing of the instrument can be accomplished in order to observe the solar disc. In this case a neutral density filter can be used to attenuate strong fluxes. For stray light suppression purposes the optical layout of the three telescopes consists of an entrance aperture, a sun light trap inside the instrument, and an adjustable internal occulter. The entrance aperture acts as an external occulter, the sun light trap intercepts direct solar radiation entering the entrance aperture, while an internal occulter masks the primary mirrors and prevents the light of the solar disc, diffracted by the external occulter, from being reflected and imaged inside the spectrometer. An analysis of the stray light properties of UVCS and of the optical performances of the spectrometer and the whole instrument are given in Romoli et al. (1993), Pernechele et al. (1997), Gardner et al. (1996).

1.3. The observations

The data on which this work is based have been acquired during the period 5–11 August 1996. We observed the North-East sector of the solar corona at $1.5\ R_\odot$, taking exposures on successive days at 0, 90, and 30, 60 degrees of Roll-angle (0 and 90 deg correspond to the East and the North direction, respectively), thus covering the sector at four latitudes in two days. Slit widths of $50\ \mu$m for the Ly α channel and $75\ \mu$m for the O VI one have been selected to optimize both spectral resolution and photon flux. The exposure times were 9000, 14400, 18000 and 25200 s, respectively for 0, 30, 60 and 90 deg, and each observation consists of a series of consecutive 600 s exposures. Different points of the spectral image along the slit (40 arcmin of length) correspond to different heliocentric distances. This allowed us to obtain FWHM values from 1.5 $R_\odot$ (from regions about the slit center), up to 2.0 $R_\odot$ for the Ly α channel, and up to 1.9 $R_\odot$ for the O VI one (from regions at the slit edges). Spatial information has been binned over 6 pix, each bin corresponding to 42 arcsec, while the spectral bin has been kept 1 detector pixel wide (the spectral bandwidth of pixel at the $1^{\rm st}$ order being 0.14 Å for the Ly α channel and 0.0925 Å for the O VI one) to have a good spectral resolution while covering a relatively wide spectral range. In fact, the total number of spectral and spatial bins available in the adopted detector mask is limited. Our observations are complemented by the daily synoptic program, which makes a complete latitudinal and radial (1.5–3.0 $R_\odot$) scan of the corona. The synoptic observations basically give information on the solar corona intensity in different UV spectral lines (e.g. H I Ly α and Ly β, O VI, Mg X, Si XII). In these, the spectral resolution of the O VI channel is relatively low, while that of the Ly α is quite good. However, these latter had a lower signal to noise ratio compared to our dedicated observations.

2. Data reduction

The main parameters characterizing a spectral line profile are its subtended area and shape. The former corresponds to the intensity integrated over the exposure time and is related, through the calibrated sensitivity of the instrument, to the photon flux from the corona. The latter is mainly related to thermal and non-thermal motions, which cause both a broadening and a shift of the line profile. Furthermore, the recorded spectral line profile can be affected by a few instrumental effects. First, it can be broadened by the finite instrumental resolution; second, it can be modified by additional spurious contributions from chromospheric radiation (recorded as stray light in the instrument)

and from interplanetary emission. The instrumental function has been determined on the basis of laboratory tests, performed during the instrument calibration ground activity, and of in flight observations of narrow chromospheric lines. It has been estimated to have a FWHM of 0.28 Å in the Ly α channel and of 0.18 Å in the O VI one, and to scale with the width of the slit, approximatively as given by the convolution of gaussian profiles (Gardner et al. 1996). A further correction is due to the presence of broad line wings in the observed profiles. This instrument characteristic has been removed by deconvolving the observed profiles with a proper zero integral function (Kohl et al. 1997). The stray light contribution has been evaluated from the observation of typical low excitation chromospheric lines, which, in spite of not being generated in the corona, appear in the recorded spectra. Because the solar disc has not been sistematically observed with UVCS, in order to estimate the stray light contribution we used disc observations of Ly α, Ly β at 1025.7 Å, O VI, Si XII at 1041.2 Å (520.6×2), and Si III at 1206.5 Å, performed in October and November 1996, under the hypothesis that the emission was stable over the 4–5 months period since our observations have been made. The Si III line, which is visible in the Ly α channel, has been used as a diagnostic tool for both UVCS channels, since no useful diagnostic line have been detected in the O VI one. So, the stray light contribution has been assumed to be essentially the same in the two channels, as they are virtually identical. The C II chromospheric line at 1037.0 Å, appearing on the wing of the O VI line at 1037.6 Å, is too faint and blended to be used as a reliable indicator of stray light. Nevertheless, a tentative estimate of its intensity is in reasonable agreement with the above assumption. Averaging along the slit the disc intensities of Ly α, Ly β, O VI, Si III, and Si XII, we obtained the following ratios: $I_{\mathrm{Ly}\ \alpha}/I_{\mathrm{Si\ III}} = 126.1$, $I_{\mathrm{Ly}\ \beta}/I_{\mathrm{Si\ III}} = 3.6$, $I_{\mathrm{O\ VI\ 1032}}/I_{\mathrm{Si\ III}} = 2.6$, $I_{\mathrm{O\ VI\ 1037}}/I_{\mathrm{Si\ III}} = 1.2$, and $I_{\mathrm{Si\ XII}}/I_{\mathrm{Si\ III}} = 0.02$.

We note a discrepancy between the ratio of the disc intensities $I_{\mathrm{Ly}\ \alpha}/I_{\mathrm{O\ VI\ 1032}}$ derived from UVCS observations, and that reported by Wilhelm et al. 1998, obtained by the SUMER/SOHO experiment. A discussion on this point and its consequences on the determination of the stray light contribution is given in Sect. 3, together with an analysis of the errors in the data reduction procedure.

A comparison between the Si III line profile observed on the solar disc and the Si III coronal line profiles showed some small line broadening, attributable to the neutral density filter inserted in the Ly α channel for disc observations. From this we estimated the correction to be applied to the observed chromospheric Ly α profile in order to recover the real one. It is interesting to compare the FWHM we have derived from UVCS disc data with that measured by SUMER on the september 15, 1998 (Lemaire et al. 1998). The profile we have observed shows roughly a gaussian shape with a relatively flat top and $\mathrm{FWHM} \approx 0.94$ Å. The saturated maximum can be indicative of self-absorbed profile. Indeed, the SUMER observation, taken with higher spectral resolution, shows a self-reversed profile, with the two peaks about 0.45 Å apart, and $\mathrm{FWHM} \approx 0.85$ Å, essentially in agreement with our observations.

Table 1. Parameters of relevant stray light lines.

line	I (ph s^{-1} cm^{-2} sr^{-1})	FWHM (Å)
Ly α	$3.2 \cdot 10^{10}$	0.94
Ly β	$1.4 \cdot 10^{9}$	0.81
O VI 1032 Å	$7.2 \cdot 10^{8}$	0.25
O VI 1037 Å	$3.3 \cdot 10^{8}$	0.27
Si XII 1041 Å	$4.6 \cdot 10^{6}$	0.14

The stray light lines appearing in the coronal spectra turned out to be barely distinguishable from the background, i.e. they have a very low signal to noise ratio. Consequently, stray light estimates have been derived averaging along the slit and over our entire observational set, assuming an overall constancy of the corresponding contributions at different latitudes. In Table 1 the derived intensities and the FWHM values are given, corrected for the described instrumental effects, for the chromospheric stray light components of Ly α, Ly β, O VI, and Si XII. The values of Table 1 have been used to correct the coronal profiles for the stray light contribution. The resulting profile has been fitted by a gaussian shape minimizing the χ-square values, and then corrected for the slit width.

Finally, the contribution from the interplanetary emission turned out to be altogether negligible, at least for heliocentric distances lower than $\sim 2\ \mathrm{R}_{\odot}$, independently of the latitude, being the expected value of the order of 3×10^{7} ph s^{-1} cm^{-2} sr^{-1} (Kohl et al. 1997).

3. Error analysis

The major sources of uncertainty in the analysis we described are: i) uncertainties in the estimate of the stray light contribution; ii) the flat-field correction; iii) uncertainties in the instrumental function; iv) errors in the line fitting procedure; v) fluctuations of the coronal emissions.

3.1. Stray light contribution

The determination of the stray light contribution is mainly affected by the uncertainty in the measure of the line intensity ratios on the solar disc. A possible explanation of the discrepancy of the UVCS results with those obtained by SUMER (see Sect. 2) can be found in the uncertainty on the knowledge of the UVCS slit width when using a narrow slit to observe the solar disc. Another possible source of uncertainty is the relative calibration between the Ly α and O VI channels. In this case the stray light correction will not be affected, since it is derived from line intensity ratios relative to observations in the same channel. Finally, we note that our measures of the disc line intensities are relative to the emission integrated over the whole solar disc, while SUMER observations refer to a region near the Sun center.

Another source of error in the stray light evaluation, is the uncertainty in the measure of the Si III line intensities in the coronal spectra. We estimated this error by gathering arbitrarily

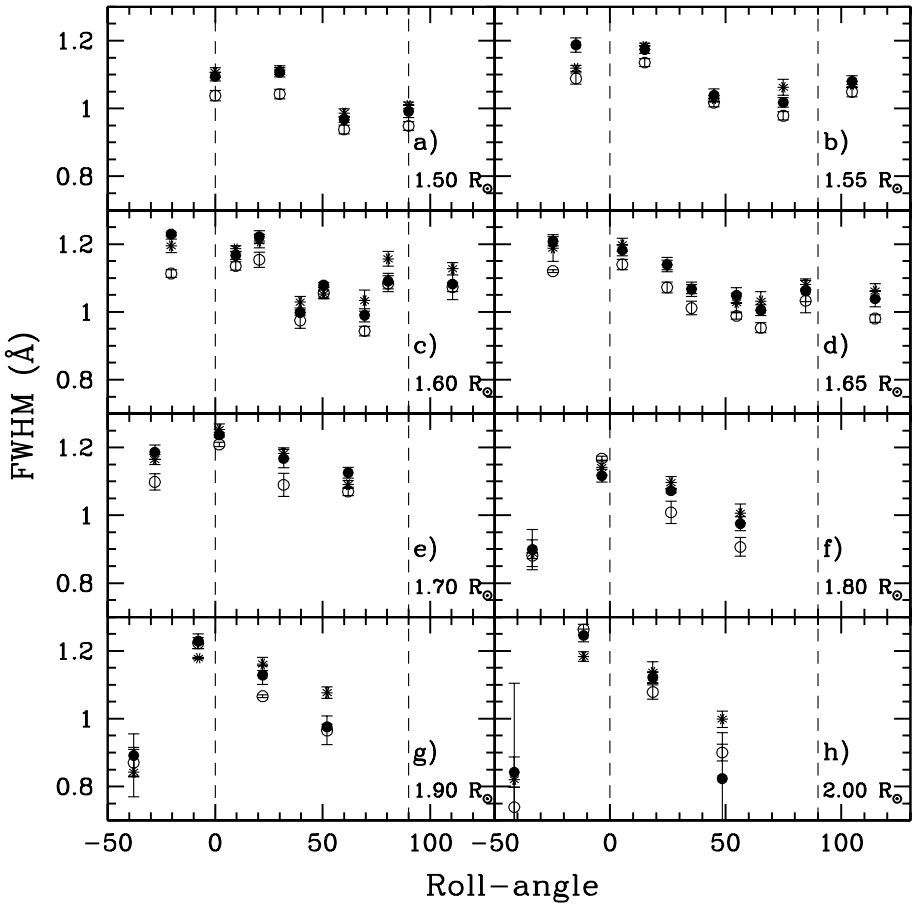

Fig. 1a–h. Line widths of the Ly α spectral line vs. Roll-angle, for different heliocentric distances. The open circles represent the first couple of days, full circles the second one, and the asterisks the third couple. The vertical dashed lines mark the equator at East (0) and the North pole (90).

into three groups all the available observations of the Si III line, so obtaining three values for its intensity. The resulting variance is 3.4% of the mean value. However, from other observations at 1.5 $R_\odot$ the intensity of the Si III line turns out to vary by a factor of 2–3 in a few week time period. This uncertainty in the stray light correction may affect noticeably the observed O VI line profiles, especially those at higher heliocentric distances, i.e. corresponding to the edges of the spectrometer slit. In these cases the resulting FWHMs can vary by more than a factor of 2 for a similar change in the stray light subtraction, as in the case of the O VI at 1037.6 Å, and even lead to slightly self-reversed profiles. This issue and the corresponding physical meaning need further careful evaluation. Measures taken in the central region of the slit are far less affected by the uncertainty in the stray light correction. In addition, as previously discussed, we are assuming that the measures of the chromospheric emission are representative of the conditions of the solar disc during the observations, although they have been performed a few months later.

3.2. Flat-field correction

The acquired spectra have been corrected also for the non uniform response of the detector, induced by variations of the detection efficiency across the sensitive surface of the MCP. For this correction, since the observations have been performed in the early phase of UVCS operational life, the flat-field response determined during the pre-launch test and calibration campaign has been used, under the assumption that it was essentially unchanged.

In the laboratory tests, it has been verified that the response was uniform within 20% (Siegmund et al. 1994). We point out that the uniformity of the detection efficiency can be modified by prolonged exposures to relatively high fluxes of parts of the detector sensitive area. However, for reducing this effect, care has been taken of shifting the spectrum from time to time, in order to expose different portions of the photocathode.

3.3. Instrumental function

The uncertainty in the width of the spectral instrumental function has been estimated to be 0.042 Å in the Ly α channel and 0.002 Å in the O VI one (Gardner et al. 1996), corresponding to $\sim 3\%$ and $\sim 1\%$ of typical line width values, respectively. The correction for the line wings tends to give narrower profiles. The corresponding change of the FWHM values is about 12% in the case of Ly α, and 15–20% for the O VI lines at 1031.9 Å and 1037.6 Å. The error in the coefficients of the zero integral function used to remove this instrument characteristic is of the order of 30%, giving an uncertainty of the resulting width for the line wing correction of 4% for Ly α, and 5–6% in the case of O VI lines. The resulting global uncertainty in the FWHM

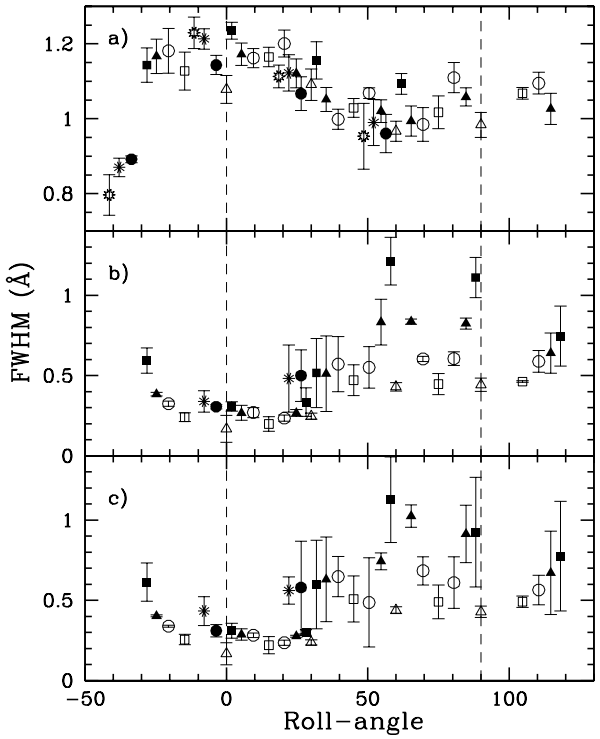

Fig. 2a–c. Comprehensive representation of the latitude behaviour of the line widths vs. Roll-angle for Ly α (panel **a**), O VI at 1031.9 Å (panel **b**), and O VI at 1037.6 Å (panel **c**), integrated over the whole observational week. Open triangles represent values at 1.5 $R_\odot$, open squares at 1.55 $R_\odot$, open circles at 1.6 $R_\odot$, full triangles are relative to values at 1.65 $R_\odot$, full squares at 1.7 $R_\odot$, full circles at 1.8 $R_\odot$, asterisks at 1.9 $R_\odot$, and stars at 2.0 $R_\odot$.

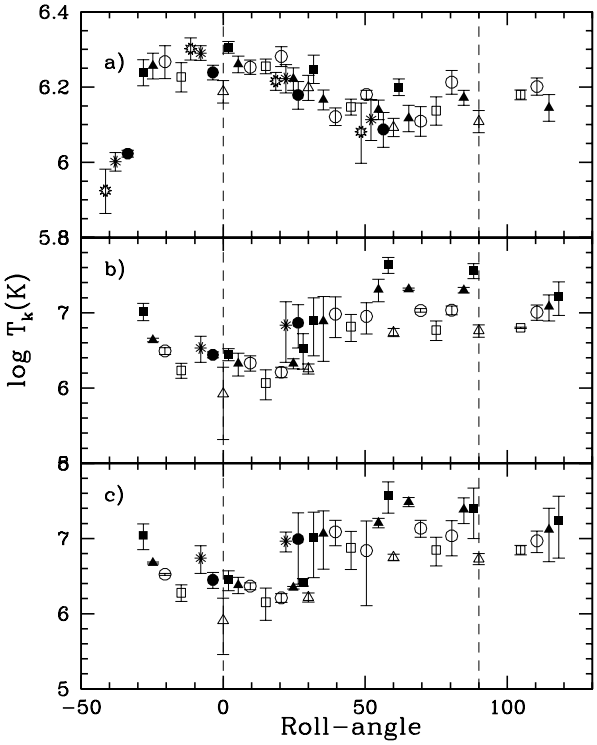

Fig. 3a–c. Kinetic temperature vs. Roll-angle for the data shown in Fig. 2, with the same meaning of the symbols.

measure introduced by the instrumental function is about 7% for both Ly α and O VI.

3.4. Fit procedure

The errors introduced by the gaussian fit of the observed profiles can be estimated by randomly varying the counts along the spectral profile within the variance given by the poissonian statistics. We obtained that the error in the FWHM values, at all latitudes and heliocentric distances, for Ly α is always $\sim 0.5\%$, and for O VI at 1031.9 Å is about 2–4%, while in the case of O VI at 1037.6 Å the variation is about 3% at low heliocentric distances and 30% for polar latitudes at high heliocentric distances.

3.5. Fluctuations of the coronal emission

In order to obtain a good statistics with mean values representative of the local conditions in the corona, the spectral profiles of the observations have been summed over 5 spatial bins, i.e. 30 pix. The corresponding radial extension of the probed region is ± 0.02 $R_\odot$ in the central region of the slit (1.5 $R_\odot$), and ± 0.06 $R_\odot$ at the edge (1.8 $R_\odot$).

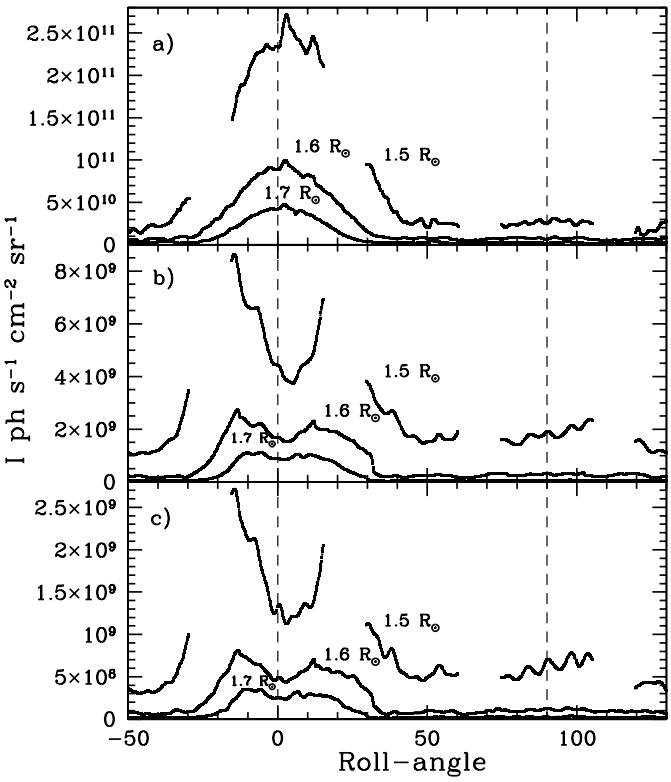

Fig. 4a–c. Intensity profile vs. Roll-angle for Ly α (panel **a**), O VI at 1031.9 Å (panel **b**), and O VI at 1037.6 Å (panel **c**), for the three heliocentric distances 1.5, 1.6, and 1.7 $R_\odot$.

To evaluate the influence of the variations in the coronal emission during the observations, we arbitrarily gathered the exposures of each day of observation into three groups, and measured the FWHM values for each group. The corresponding sigma values are shown as bars in the figures presented in this paper, and include the uncertainty introduced by the fitting procedure.

We point out that the error sources discussed in Sects. 3.1 and 3.3 should affect measurements in an almost systematic way, and in case shift all data in Figs. 1, 2, 5, and 6 by a small Δ FWHM amount. In fact, as previously discussed, the errors introduced by the correction for the instrumental function are about 7% for both channels. Moreover, we tested the errors introduced by the stray light correction subtracting $1/2$ and $1/3$ of the contribution estimated from our analysis (we have some indication that we somewhat overestimated the stray light contribution by a factor of 2). Subtracting $1/2$ of the estimated stray light, it turns out that almost all data points are lowered by a fixed amount (about 0.02 Å for the Ly α and 0.1–0.2 Å for the O VI profiles), except those of O VI at distances higher than $1.6\ \mathrm{R}_\odot$, for which the shift is about 0.5 Å. The result is that the stray light subtraction tends to broaden the O VI line profiles more significantly at higher latitudes. However, we point out that the qualitative behaviour of the these profiles with latitude (see the following discussion in Sect. 4) is not modified by this uncertainty. The subtraction of $1/3$ of the stray light gives results similar to the former case. On the basis of these considerations, excursions of the measured quantities larger than the error bars are expected to be physically significant fluctuations in the measured FWHMs.

4. Discussion

In Fig. 1 the temporal evolution of the FWHM values of the Ly α spectral profiles is reported vs. Roll-angle for different heliocentric distances, from 1.5 up to $2.0\ \mathrm{R}_\odot$. In each panel the values relative to the observations in the three different couple of days, for a fixed distance, are shown. The most prominent feature that can be appreciated, is the presence, in the streamer region, of relatively wide profiles, which become narrower towards higher latitudes. This tendency becomes more evident in measures taken at higher distances. This behaviour of the Ly α line profile, which is in contrast to that of O VI (see the discussion below), had not been put clearly in evidence previously, to our knowledge. Preliminary results based on synoptic observations, claiming for Lyα profiles somewhat wider in the streamer region, have been presented by Strachan et al. (1997). We can also notice how the FWHM values globally increase with time, expecially passing from the first to the second couple of days of observation. In fact, data points represented by open circles, which are relative to the first couple of days, are systematically lower than full circles (second couple of days), and the latter are lower than asterisks (third couple of days). This fact is less clear in measures corresponding to high distances (1.9–$2.0\ \mathrm{R}_\odot$), owing to larger errors in the determinations. We did not find a clear correlation between the temporal evolution of the line profiles and the corresponding line intensity behaviour.

The more outstanding properties of the Ly α profiles are summarized in Fig. 2a (Fig. 2b and Fig. 2c refer to O VI at 1031.9 Å and 1037.6 Å, respectively), which gives the FWHM vs. latitude profile for data integrated over the whole week. In addition to the above stressed properties, the data show line widths slightly increasing with the distance. The corresponding kinetic temperatures are shown in Fig. 3a (Fig. 3b and Fig. 3c are relative to O VI at 1031.9 Å and 1037.6 Å, respectively), evaluated according to Eq. 1 and neglecting the contribution from non-thermal motions. The variations of the kinetic temperatures between the pole and the equator amount to about a factor of 1.3, for Ly α, with the polar kinetic temperature lower than the equatorial one.

From the analysis of the spectra taken in the O VI channel, we obtained few data for the Ly β line at 1025.7 Å. The measured line widths turn out to be equal, within the experimental uncertainty, to the corresponding values for Ly α.

For reference purposes the Ly α intensity vs. latitude profile is shown in Fig. 4a, together with the intensity profiles of O VI at 1031.9 Å (Fig. 4b) and 1037.6 Å (Fig. 4c), at three heliocentric distances: 1.5, 1.6, and $1.7\ \mathrm{R}_\odot$. It was derived from the synoptic observations by interpolating data taken at different latitudes and heliocentric distances, and has a higher spatial resolution than that achievable on the basis of our observations. In this figure streamers appear as elongated structures – with the axis roughly in the equatorial plane – which extend approximatively between -30 and $+30$ deg of Roll-angle. The Ly α emission is globally homogeneous showing a typical cusp configuration in correspondence of the equatorial current sheet, with the intensity decreasing with both latitude and heliocentric distance. A comparison with Fig. 1 reveals, over all latitudes, a correlation between the line widths and the intensity with the latitude, both of them decreasing towards the North pole. No particular correlation appears in the radial direction.

Figs. 5 and 6 show the same parameters as Fig. 1, respectively for the O VI lines at 1031.9 Å and 1037.6 Å. The larger spread of data in Fig. 6 is a consequence of the poorer statistics for the line at 1037.6 Å. The data relative to O VI have a different behaviour, both in intensity and in line width, from that shown by the previously described Ly α line. The coronal emission in the streamer region (see Figs. 4b and 4c) exhibits a double peaked spatial configuration with a deep minimum at the center of it. The comparison of the line widths shown in Figs. 5, 6 with the intensity derived from the synoptic observations shows that the narrowest values of FWHM of the line profiles are in correspondence with the minimum of intensity at the center of the streamer region. Then the decrease of intensity at the streamer boundary (at about 20–30 deg) corresponds to an increase of the line widths. Moving towards the North pole we can appreciate an almost steady increase of the line widths with latitude at any heliocentric distance. Moreover, data relative to higher distances are sistematically wider than those at lower distances. The line width behaviour is just the opposite to that of the line intensity, which decreases both with latitude and distance. We did not find evidence for a particular behaviour in correspondence with the double peak in intensity at about -20 and $+20$ deg. The corresponding kinetic temperatures are

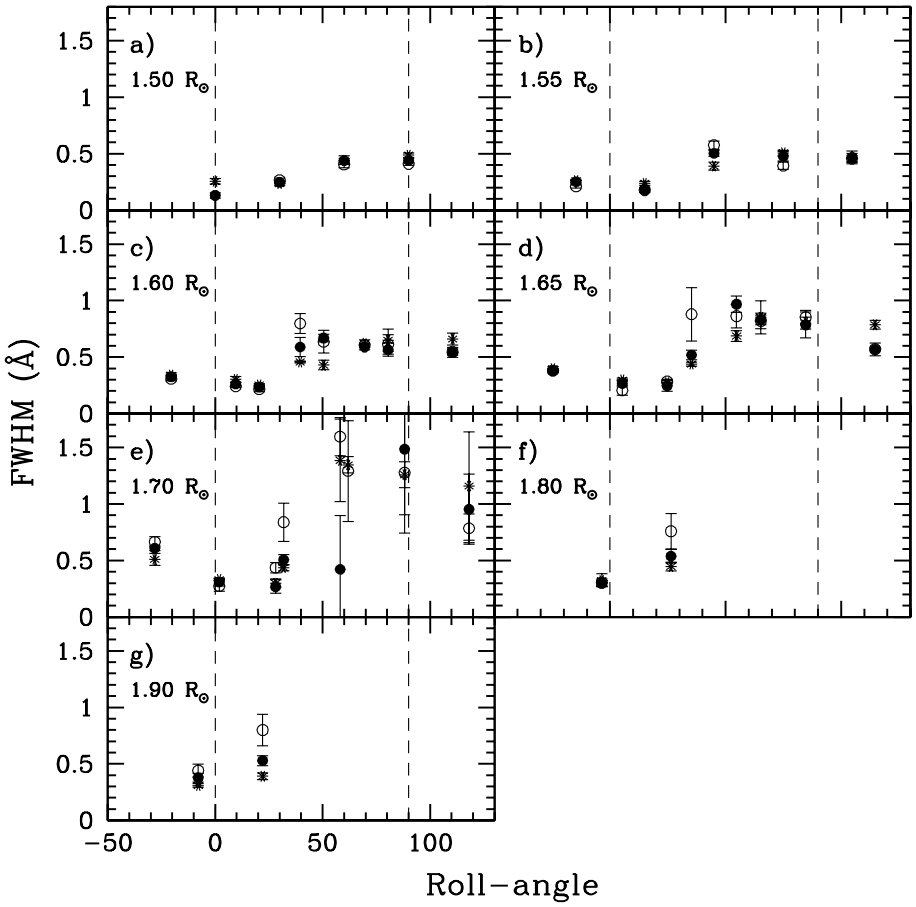

Fig. 5a–g. The same representation as in Fig. 1 but for the O VI line at 1031.9 Å, with the same meaning of the symbols.

shown in Figs. 3b and 3c. The measures taken at the equator are lower than those relative to the pole, and differ by a factor of 10.

Kohl et al. (1997), Noci et al. (1997a), and Antonucci et al. (1997) have already noticed that the O VI root mean square (r.m.s.) velocity measured along the instrument slit increases, as we move out of the equatorial streamer. However, Noci et al. (1997a) and Antonucci et al. (1997) give the O VI r.m.s. velocity vs. position along the slit, and it is not straightforward to identify separately the latitudinal and the radial effect. These authors also put in evidence the anticorrelation between the r.m.s. velocity of O VI and the line intensity. Strachan et al. (1997) have shown the behaviour of O VI line profiles as a function of latitude, using observations at low spectral resolution, confirming the presence of narrow profiles in the streamer region.

The most striking feature that can be appreciated by comparing Figs. 1, 4, 5, and 6, is the different behaviour between the Ly α and the O VI profiles, the Ly α showing wider profiles inside the streamer region, where the O VI profiles, on the contrary, present a deep minimum. Moreover, the O VI line widths tend to increase with latitude, while the width of the Ly α profiles decreases outside the streamer to about 50–60 deg, then slightly increase towards the North pole. All the described features do not show significant variations in time, as can be seen by looking at the different panels of Figs. 1, 5, and 6, at least within one week of observations.

This work represents a systematic analysis of the variation of the line widths with latitude and heliocentric distance, in the range 1.5–2.0 $R_\odot$. Some indications on the expected behaviour of these parameters may be found in the quoted literature. Recent UVCS observations (Kohl et al. 1998) revealed that the coronal heating mechanism has two main properties: i) higher mass ions are preferentially heated; ii) the mechanism operates more efficiently in the normal than in the radial direction. This two characteristics suggest that high frequency Alfvén waves dissipation via ion-cyclotron resonance damping (McKenzie, Axford, & Banaszkiewicz 1997; Tu & Marsh 1997; Marsh & Tu 1997) may be responsible for the observed phenomena.

In the ion-cyclotron resonance damping scenario we expect larger line widths where the ion-cyclotron resonance damping is more efficient. Ulysses observations have revealed that Alfvén waves are continuously present in the polar region of the sun while at lower latitudes they become increasingly scarce and intermittent (Smith et al. 1995). The behaviour of the O VI profiles shown in Figs. 5, 6 is consistent with the ion-cyclotron coronal heating interpretation and the behaviour of the Alfvén waves with latitude, as we expect wider profiles in the polar region, where Alfvén waves have been continuously observed. The results for Ly α, however, are apparently inconsistent with this scenario, as narrower profiles are seen in the polar region. However, we point out that the ion-cyclotron mechanism is much less efficient for lower mass ions; hence we can hypothesize that for

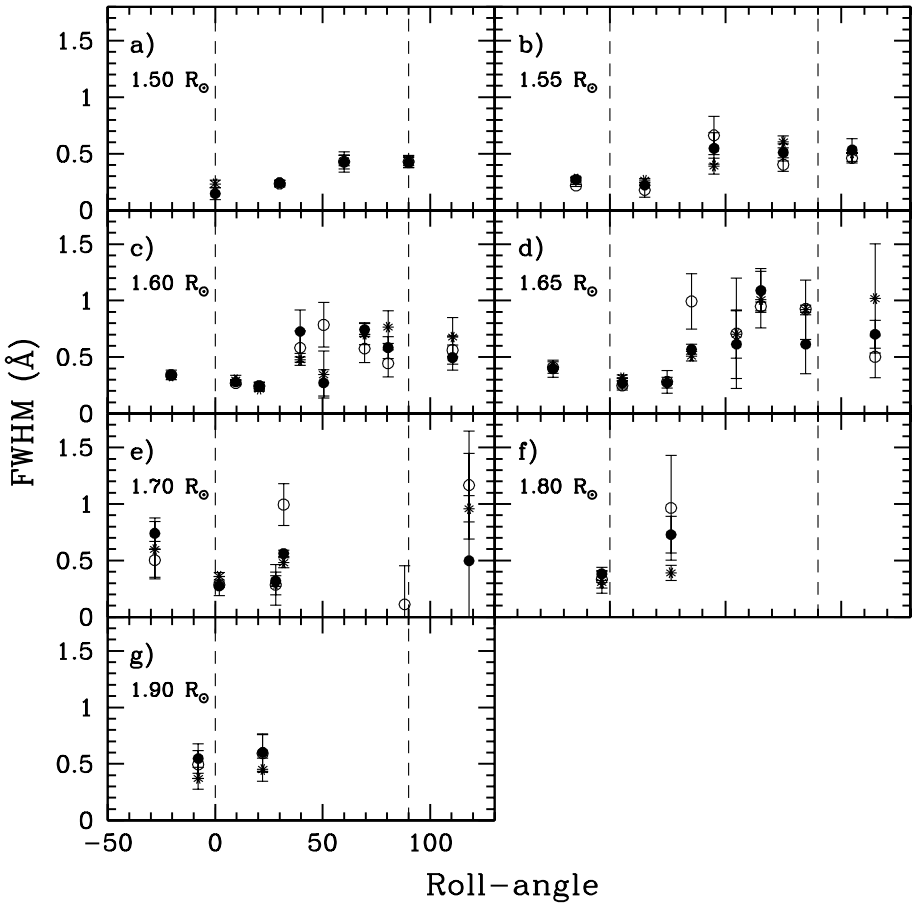

Fig. 6a–g. The same representation as in Fig. 1 but for the O VI line at 1037.6 Å, with the same meaning of the symbols.

the protons it is masked by other effects. The phenomenon of the decrease of the Ly α line widths towards the pole, in contrast with the opposite behaviour of O VI, appears to us to be an important constraint for theoretical models of coronal heating.

We looked for consistency with the ion-cyclotron scenario also by analyzing some measurements for the profile of the Si XII line at 1041.2 Å. Owing to the poor statistics we integrated the data over the whole week, obtaining width values only for the center of the streamer (a region between -4 and 10 deg across the equator), and for the border of it (between 20 and 30 deg). In Fig. 7 the corresponding kinetic temperature for the Si XII line is shown as a function of the heliocentric distance, compared with the analogous data points for O VI line at 1031.9 Å. In the center of the streamer (Fig. 7a) and at its border (Fig. 7b) the kinetic temperature of Si XII appears to be larger than the O VI one. The interpretation of this behaviour is not immediate, because we would expect $T_{\rm k}$ of Si XII to be lower than that of O VI, at least in regions where the ion-cyclotron mechanism is effective. In fact, according to the ion-cyclotron mechanism theory, the efficiency of the heating process depends on the ratio *A/Z* (*A* is the atomic mass and *Z* is the ion charge), which for Si XII is lower than for O VI. Hence, we conclude that the presented analysis of Si XII lines does not allow us to make any definite conclusion about the effectiveness of the ion-cyclotron mechanism in the explored regions. Tu et al. (1998), in a recent work, have analysed the behaviour of ion temperatures as a function of the ratio *A/Z*, in a polar coronal hole, on the basis of SUMER data, and found only a very weak evidence in favour of the trend implied by the ion-cyclotron heating mechanism.

The different morphology of the streamer region in the O VI and Ly α lines has been already pointed out by Noci et al. (1997b). An interpretation of this difference in terms of a minimum in the Oxygen abundance in the central region of the streamer, where the O VI intensity is lower, has been advanced by Noci et al. (1997b), Raymond et al. (1997). If the abundance is the cause of the O VI intensity variations across the streamer, these variations do not imply corresponding changes in the line width. Our data show that this is in fact the case, and support that interpretation.

A last issue that we would like to notice is a characteristic of the FWHM of O VI line profiles vs. latitude, as it emerges from Figs. 5 and 6. Panels a, b, c, and d are possibily consistent with a bimodal behaviour of the line widths, which, within the latitude range between -30 and $+30$ deg, seem to cluster around a constant value of ~ 0.25 Å, while in the latitude range between 40 and 110 deg around a constant value of 0.5–1.0 Å (depending on the altitude of observation). Although the spatial resolution of our data is not high enough to ascertain whether line widths have a bimodal character, we point out that the rise from low to high line width values occurs in a 10 deg wide region. More detailed observations could establish whether the bimodal character seen in Ulysses wind data shows up also in the line widths.

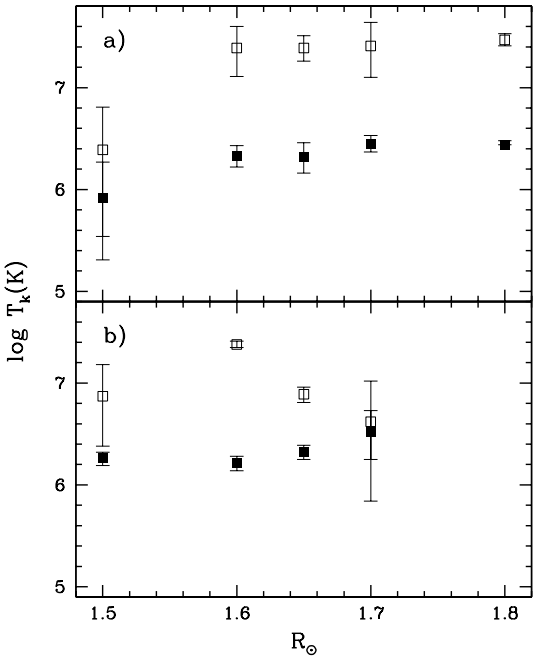

Fig. 7a and b. Kinetic temperature vs. heliocentric distance for the Si XII at 1041.2 Å (open squares) and O VI at 1031.9 Å (full squares) lines. Panel **a** is relative to the center of the streamer, while panel **b** refers to its border.

5. Conclusions

In the present study of the solar corona line profiles obtained with the UVCS experiment, we have put in evidence the properties of the UV lines Ly α and O VI as a function of the latitude and heliocentric distance. We also tried to analyse the implications of the results for the coronal heating theories, particularly with respect to the ion-cyclotron resonance damping mechanism. Data for different ions and with a higher spatial resolution are needed to study in deeper details the features enlightened in this work. A further analysis is in progress to examine whether the bimodal character of the flow speed seen by Ulysses can be detected also at the smaller altitudes probed by our observations.

Acknowledgements. The authors wish to acknowledge the support provided by ASI (Agenzia Spaziale Italiana) and NASA (National Aeronautics and Space Administration). LZ and PN are particularly indebted to Dr. G. Naletto and Dr. D. Spadaro for many helpful discussions. Moreover, LZ whishes to thank Dr. G. Corti for a first introduction to the UVCS data analysis.

References

Antonucci E., Giordano S., Benna C., et al., 1997, On Signatures of Nonthermal Particles During CME Acceleration. In: A. Wilson (ed.) Proc. Fifth SOHO Workshop, The Corona and Solar Wind Near Minimum Activity. ESA Publications Division, The Netherlands, p. 175

Domingo V., Fleck B., Poland A.I., 1995, Solar Phys. 162, 1

Gardner L.D., Kohl J.L., Daigneau P.S., et al., 1996, Proc. SPIE 2831, 2

Jefferies J.T., 1968, Spectral Line Formation. Blaisdell Publishing Company, Waltham

Kohl J.L., Esser R., Gardner L.D., et al., 1995, Solar Phys. 162, 313

Kohl J.L., Noci G., Antonucci E., et al., 1997, Solar Phys. 175, 613

Kohl J.L., Noci G., Antonucci E., et al., 1998, ApJ 501, L127

Lemaire P., Emerich C., Curdt W., Schühle U., Wilhelm K., 1998, A&A 334, 1095

Lima J.J.G., Priest E.R., 1993, A&A 268, 641

Lima J.J.G., Tsinganos K., 1996, Geophys. Res. Lett. 23, 117

Marsh E., Tu C.Y., 1997, A&A 319, L17

McKenzie J.F., Axford W.I., Banaszkiewicz M., 1997, Geophys. Res. Lett. 24, 2877

Noci G., Kohl J.L., Withbroe G.L., 1987, ApJ 315, 706

Noci G., Kohl J.L., Antonucci E., et al., 1997a, Adv. Space Res., 20, 2219

Noci G., Kohl J.L., Antonucci E., et al., 1997b, The Quiescent Corona and Slow Solar Wind. In: A. Wilson (ed.) Proc. Fifth SOHO Workshop, The Corona and Solar Wind Near Minimum Activity. ESA Publications Division, The Netherlands, p. 75

Pernechele C., Naletto G., Nicolosi P., et al., 1997, Appl. Opt. 36, 813

Phillips J.L., Bame S.J., Barnes A., et al., 1995, Geophys. Res. Lett. 22, 3301

Raymond J.C., Kohl J.L., Noci G., et al., 1997, Solar Phys. 175, 645

Romoli M., Weiser H., Gardner L.D., Kohl J.L., 1993, Appl. Opt. 32, 3559

Sauty C., Tsinganos K. 1994, A&A 287, 893

Siegmund O.H.W., Gummin M.A., Stock J., et al., 1994, Proc. SPIE 2280, 89

Smith E.J., Balogh A., Neugebauer M., McComas D., 1995, Geophys. Res. Lett. 22, 3381

Stewart G.A., Bravo S., 1997, J. Geophys. Res. 102, 11263

Strachan L., Raymond J.C., Panasyuk A.V., et al., 1997, Spectroscopic Observations of the Extended Corona During the SOHO Whole Sun Month. In: A. Wilson (ed.) Proc. Fifth SOHO Workshop, The Corona and Solar Wind Near Minimum Activity. ESA Publications Division, The Netherlands, p. 691

Tu C.Y., Marsh E., 1997, Solar Phys. 171, 363

Tu C.Y., Marsh E., Wilhelm K., Curdt W., 1998, ApJ 503, 475

Wang A.H., Wu S.T., Suess S.T., Poletto G., 1998, J. Geophys. Res. 103, 1913

Wilhelm K., Lemaire P., Dammasch I.E., et al., 1998, A&A 334, 685

Withbroe G.L., Kohl J.L., Weiser H., Munro R.H., 1982, Space Sci. Rev. 33, 17